

Figure 1 A chart of the nuclides with the black squares, representing the stable nuclei, plotted as a function of the number of protons and neutrons in the nucleus. It also shows the limits of observation of nuclei, the drip-lines and the astrophysical r- and rp-process pathways.

Secondary beams of rare isotopes

1 Introduction

The study of nuclear physics demands beams of energetic particles to induce nuclear reactions on the nuclei of target atoms. It was from this need that accelerators were born. Over the years nuclear physicists have devised many ways of accelerating charged particles to ever increasing energies. Today we have beams of all nuclei from protons to uranium ions available at energies well beyond those needed for the study of atomic nuclei. This basic research activity, driven by the desire to understand the forces which dictate the properties of nuclei, has spawned a large number of beneficial applications. Amongst its many progeny we can count reactor- and spallation-based neutron sources, synchrotron radiation sources, particle physics, materials modification by implantation, carbon dating and much more. It is an excellent example of the return to society of investment in basic research.

All of these achievements have been realized by accelerating the 283 stable or long-lived nuclear species we find here on Earth. We see them in Fig. 1, the black squares, plotted as a function of the numbers of protons (Z) and neutrons (N) that they contain. In recent years, however, it has become evident that it is now technically possible to create and accelerate unstable nuclei and, as we see in Fig. 1, there are some 6-7,000 distinct nuclear species which live long enough to be candidates for acceleration. They are the nuclei within the so-called drip-lines, the point where

the nucleus can no longer hold another particle. It needs little imagination to see that this development might not only transform Nuclear Physics but could lead to many new, undreamed of, opportunities in industry, medicine, material studies and the environment.

Fig. 2 shows schematically the two main methods of radioactive beam production which have been proposed. They are commonly known as the ISOL-Isotope separation on line - and In-flight techniques. In the ISOL method, we must first make the radioactive nuclei in a target/ion source, extract them in the form of ions and, after selection of mass by an electromagnetic device, accelerate them to the energy required for the experiments. In contrast, the in-flight method relies on energetic beams of heavy ions impinging on a thin target. Interactions with the target nuclei can result in fission or fragmentation, with the nuclei which are produced leaving the target with velocities close to those of the projectiles. A cocktail of many different species is produced which, since the ions have high velocities, does not need further acceleration to transport it to the secondary target. On route to the target the reaction products can be identified by mass, charge and momentum in a spectrometer (fragment separator). Thus a pure beam is not separated out from the cocktail. Instead each ion is tagged and identified by these primary characteristics and the secondary reactions are studied on an event-by-event basis. Another possibility is a combination of the two methods in which the in-flight reaction products are brought to rest in a gas cell, sucked out and separated by mass and then re-accelerated to the required energy. For reviews of experimental and theoretical developments involving production, acceleration, and reactions with unstable nuclei, see, e.g., Refs. [1, 2, 3, 4, 5, 6, 7, 8].

The ISOL and in-flight methods are complementary in almost every respect. With the ISOL technique one can produce beams of high quality, comparable to that of stable beams. Since we start with ions at the temperature of the target/ion source the process is similar to the way the beam is generated in a stable beam accelerator so one can produce beams of similar quality. Strong ISOL beams can be produced but the intensity varies markedly according to a) the chemical species involved and b) how far from stability they are. Refractory elements such as zirconium and molybdenum are extremely difficult to ionize and are not suitable for the method at present. This technique also relies on the diffusion and effusion of the radioactive atoms in the target, which is maintained at high temperatures ($\sim 2500^\circ\text{C}$) to speed the process up. Such diffusion processes vary a lot in speed. For short-lived nuclear species, with half-lives of milliseconds or less, this is often the limiting factor in intensity because the atoms decay before they reach the final target.

In contrast, in-flight facilities can produce all chemical species with half-lives greater than about 150ns, the time of transit through the fragment separator, and since the beams are produced at high energy they do not need re-acceleration. The main drawbacks of this method however are that a) the beams are weak, b) they are not separated physically - the individual ions are simply tagged electronically by A,

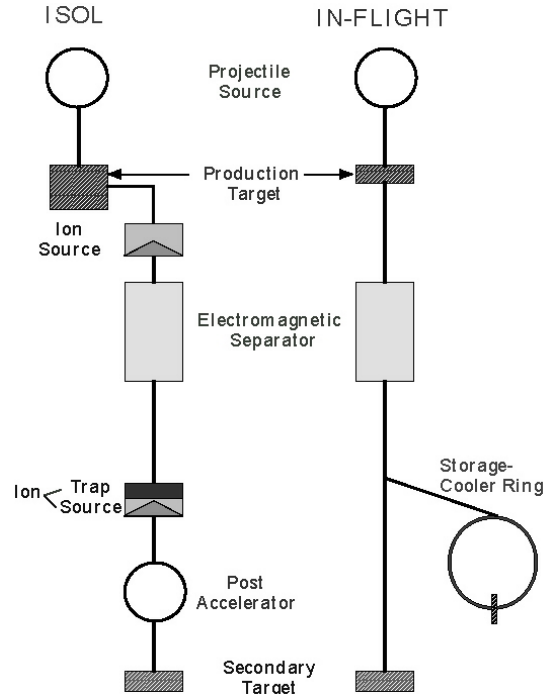


Figure 2 A schematic view of the basic methods of producing radioactive nuclear beams. At the left we see the ISOL method with and without a post-accelerator. At the right we see the In-flight method and the proposed hybrid in which fragments are caught in a gas cell and then re-accelerated.

Z and momentum and c) they are of poor quality in terms of energy and focussing.

Assume that a highly energetic uranium projectile ($N/Z \sim 1.6$) hits a target nucleus in an almost central collision, as shown in Fig. 3. A part of the projectile (participant) is scrapped off and forms a highly excited mixture of nucleons with a part of the target. A piece of the projectile (spectator) flies away with nearly the same velocity of the beam. The neutron-to-proton-ratio of the spectator is nearly equal to that of the projectile. Since the N/Z - ratio of light nuclei (stable) is close to one, the fragment is far from the stability line. Statistically, a large number of fragments with different N/Z - ratios is created and several new exotic nuclei have been discovered in this way.

Experiments with secondary-beam are limited by reaction cross section and luminosity. The luminosity L is defined as the product of beam intensity i and target thickness t :

$$L = i \cdot t. \quad (1)$$

The reaction rate N is the product of luminosity and reaction cross section σ_r :

$$N = \sigma_r \cdot L. \quad (2)$$

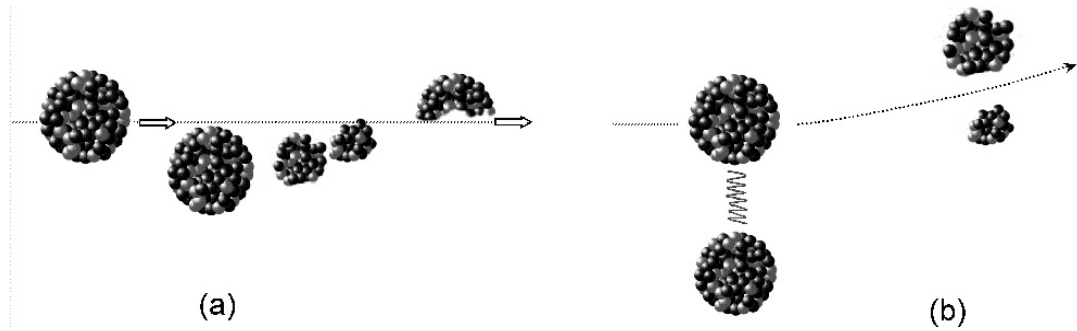


Figure 3 (a) Schematic description of a nuclear fragmentation reaction producing rare isotopes. The lower fragments are called participants, while the upper one is called by spectator. Using uranium projectiles ($N/Z \sim 1.6$) one expects to produce (light) spectator nuclei of about the same N/Z ratio. (b) Coulomb fission of relativistic projectiles leading to the production of rare isotopes. For a heavy unstable projectile an exchanged photon with the target can give it enough energy to fragment into several types of isotopes.

In most of the reactions the usable target thickness is limited by the width of the excitation function (i.e., the cross section as a function of the excitation energy). Production reactions with a wide excitation function covering a broad energy range can profit in luminosity by the use of thick targets.

The condition for fragmentation of heavy ions is that the projectile should move faster than the nucleons move inside the nucleus. The projectile energy should be sufficiently above the Fermi domain, e.g., above 100 A MeV. The usable target thickness for these high energies is of the order of several grams per square centimeter, corresponding to $10^{23} atoms/cm^2$. The excitation function for complete fusion of heavy ions, however, has a width of only 10 MeV. This corresponds to a usable target thickness of the order of one milligram per square centimeter or $10^{18} atoms/cm^2$. Consequently beam intensities for the investigation of complete fusion reactions must be by four to five orders higher to achieve the same luminosity as for fragmentation.

Fig. 4 shows as an example the production cross sections for the tin isotopes from complete fusion (dotted line), nuclear fragmentation (solid line), and Coulomb fission of ^{238}U (dashed line). The symbols represent experimental data. The fragmentation cross-sections (solid line) have been calculated with a semi-empirical code [10].

It is very pedagogical and useful at his stage to discuss the production of nuclei in the nuclear fragmentation region of Fig. 4. We develop some mathematical tools to understand them. The simplest theoretical model to describe the isotopic distribution of fragments in heavy ion collisions at high energies is the *abrasion-ablation* one of [11]. In the model's abrasion stage, the nucleons in the overlap volume of two energetic heavy ions are scrapped off (abraded) as the ions pass each other. In

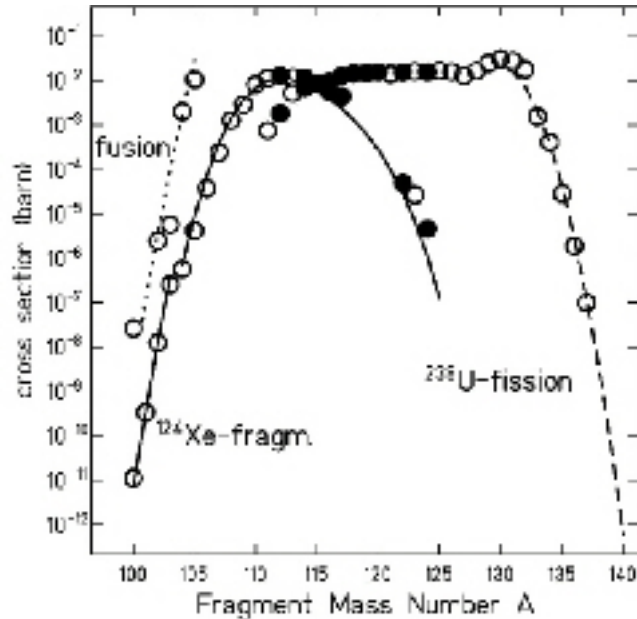


Figure 4 Production cross sections for the tin isotopes from complete fusion (dotted line), fragmentation (solid line), and projectile fission of ^{238}U (dashed line). The symbols represent experimental data. The fragmentation cross-sections (solid line) have been calculated with a semi-empirical code [10].

the subsequent ablation stage, the excited projectile and target fragments decay by emitting particles. The abrasion stage can be well described within the probability model of nuclear scattering [12, 13, 14, 15, 16].

Supplement A

2 Probability approach to high energy scattering

In this Supplement we show that most equations used in the description of nuclear fragmentation in high energy collisions can be deduced from very simple probability arguments. Let us assume, as shown in Fig. 5(a), that a nucleus-nucleus collision occurs at an impact parameter b . We can define the probability of having a nucleon-nucleon collision within the transverse element area $d\mathbf{b}$ as $t(\mathbf{b}) d\mathbf{b}$, where $t(\mathbf{b})$ is known as the *thickness function*. It is defined in a normalized way, i.e.,

$$\int t(\mathbf{b}) d\mathbf{b} = 1. \quad (3)$$

For unpolarized projectiles $t(\mathbf{b}) = t(b)$. In most practical situations one can use $t(\mathbf{b}) \simeq \delta(\mathbf{b})$, which simplifies the calculations considerably.

Since the total transverse area for nucleon-nucleon collisions is given by σ_{NN} , the probability of having an inelastic nucleon-nucleon collision is given by $t(\mathbf{b}) \sigma_{NN}$.

The probability of finding a nucleon in $d\mathbf{b}_B dz_B$ is given by $\rho(\mathbf{b}_B, z_B) d\mathbf{b}_B dz_B$, where the nuclear density is normalized to unity:

$$\int \rho(\mathbf{b}_B, z_B) d\mathbf{b}_B dz_B = 1 . \quad (4)$$

Using these definitions, it is easy to verify that the probability dP of occurrence of a nucleon-nucleon collision is given by

$$dP = \rho(\mathbf{b}_B, z_B) d\mathbf{b}_B dz_B \cdot \rho(\mathbf{b}_A, z_A) d\mathbf{b}_A dz_A \cdot t(\mathbf{b} - \mathbf{b}_A - \mathbf{b}_B) . \quad (5)$$

Thus, as in the case of free nucleon-nucleon collisions, we define $T(\mathbf{b}) \sigma_{NN}$ as the probability of occurrence of a nucleon-nucleon collision in nucleus-nucleus collisions at impact parameter b . This is obtained by multiplying dP by σ_{NN} and integrating it over all the projectile and target volumes, i.e.,

$$T(\mathbf{b}) \sigma_{NN} = \int \rho(\mathbf{b}_B, z_B) d\mathbf{b}_B dz_B \rho(\mathbf{b}_A, z_A) d\mathbf{b}_A dz_A t(\mathbf{b} - \mathbf{b}_A - \mathbf{b}_B) \sigma_{NN} . \quad (6)$$

The thickness function for nucleus-nucleus collisions, $T(\mathbf{b})$, can thus be related to the corresponding thickness function for nucleon-nucleon collisions as

$$T(\mathbf{b}) = \int \rho(\mathbf{b}_B, z_B) d\mathbf{b}_B dz_B \rho(\mathbf{b}_A, z_A) d\mathbf{b}_A dz_A t(\mathbf{b} - \mathbf{b}_A - \mathbf{b}_B) . \quad (7)$$

We notice that our definition immediately implies that $T(\mathbf{b})$ is also normalized to unity:

$$\int T(\mathbf{b}) d\mathbf{b} = 1 . \quad (8)$$

We can also define the individual thickness functions for each nucleus. That is, for nucleus A ,

$$T_A(\mathbf{b}_A) = \int \rho(\mathbf{b}_A, z_A) dz_A , \quad (9)$$

and similarly for the nucleus B . In terms of these definitions

$$T(\mathbf{b}) = \int d\mathbf{b}_A d\mathbf{b}_B T_A(\mathbf{b}_A) T_B(\mathbf{b}_B) t(\mathbf{b} - \mathbf{b}_A - \mathbf{b}_B) . \quad (10)$$

Now we are able to describe more specific aspects of nucleus-nucleus collisions in terms of nucleon-nucleon collisions. For example, we may want to calculate the probability of occurrence of n nucleon-nucleon collisions in a nucleus-nucleus collision at impact parameter \mathbf{b} . If for simplicity we call $A(B)$ the number of nucleons in nucleus $A(B)$, this probability is given by

$$P(n, \mathbf{b}) = \binom{AB}{n} [T(\mathbf{b}) \sigma_{NN}]^n [1 - T(\mathbf{b}) \sigma_{NN}]^{AB-n} . \quad (11)$$

The first term is the number of combinations for finding n collisions out of AB possible nucleon-nucleon encounters. The second term is the probability of having exact n collisions, while the last term is the probability of having $AB - n$ misses. The total probability, or differential cross section, is given by

$$\frac{d\sigma}{d\mathbf{b}} = \sum_{n=1}^{AB} P(n, \mathbf{b}) = 1 - [1 - T(\mathbf{b}) \sigma_{NN}]^{AB}, \quad (12)$$

and the total nucleus-nucleus cross section is given by

$$\sigma = \int db \left\{ 1 - [1 - T(\mathbf{b}) \sigma_{NN}]^{AB} \right\}. \quad (13)$$

For nucleus-nucleus collisions one may ask what is the average number of nucleon-nucleon collisions at a given impact parameter \mathbf{b} . One has

$$\begin{aligned} \langle n(\mathbf{b}) \rangle &= \sum_{n=0}^{AB} n P(n, \mathbf{b}) = \sum_{n=0}^{AB} n \binom{AB}{n} [T(\mathbf{b}) \sigma_{NN}]^n [1 - T(\mathbf{b}) \sigma_{NN}]^{AB-n} \\ &= \alpha \frac{\partial}{\partial \alpha} \sum_{n=0}^{AB} \binom{AB}{n} [\alpha \sigma_{NN}]^n [1 - T(\mathbf{b}) \sigma_{NN}]^{AB-n} \Big|_{\alpha=T(\mathbf{b})} \\ &= \alpha \frac{\partial}{\partial \alpha} [1 - T(\mathbf{b}) \sigma_{NN} + \alpha \sigma_{NN}]^{AB} \Big|_{\alpha=T(\mathbf{b})} \\ &= \left\{ \alpha AB \sigma_{NN} [1 - T(\mathbf{b}) \sigma_{NN} + \alpha \sigma_{NN}]^{AB-1} \right\} \Big|_{\alpha=T(\mathbf{b})}, \end{aligned} \quad (14)$$

or

$$\langle n(\mathbf{b}) \rangle = AB T(\mathbf{b}) \sigma_{NN}. \quad (15)$$

One can also calculate the standard deviation in the number of nucleon-nucleon collisions. First, we need to calculate $\langle n^2(\mathbf{b}) \rangle$. One can use the same trick as in the derivation above, replacing the sum over $n^2 P(n, \mathbf{b})$ by the application of twice the operator $\alpha \partial / \partial \alpha$. The net result is

$$\langle n^2(\mathbf{b}) \rangle = AB T(\mathbf{b}) \sigma_{NN} + AB (AB - 1) [T(\mathbf{b}) \sigma_{NN}]^2. \quad (16)$$

Using 14 and 15 we find for the standard deviation

$$\langle n^2(\mathbf{b}) - \langle n(\mathbf{b}) \rangle^2 \rangle \equiv \langle n^2 \rangle - \langle n \rangle^2 = AB T(\mathbf{b}) \sigma_{NN} [1 - T(\mathbf{b})]. \quad (17)$$

It is worthwhile to apply this formalism to nucleon-nucleus collisions. In this case,

nucleon in a tube of cross section σ_{NN} at \mathbf{b}_B . It is given by $T_B(\mathbf{b}_B)\sigma_{NN}$. The probability of finding n nucleons in the same tube is

$$\binom{B}{n} [T_B(\mathbf{b}_B)\sigma_{NN}]^n [1 - T_B(\mathbf{b}_B)\sigma_{NN}]^{B-n} . \quad (21)$$

Following the same steps as in Eq. 14 we get for the average number of collisions in this tube,

$$\langle n(\mathbf{b}_B) \rangle = BT_B(\mathbf{b})\sigma_{NN} . \quad (22)$$

Thus, the probability of having n nucleons of B in a tube of cross section σ_{NN} colliding with m nucleons of A in a similar tube is given by

$$\begin{aligned} P(n, m, \mathbf{b}_A, \mathbf{b}_B) &= \int t(\mathbf{b} - \mathbf{b}_A - \mathbf{b}_B) d\mathbf{b}_A \cdot \binom{B}{n} [T_B(\mathbf{b}_B)\sigma_{NN}]^n \\ &\times [1 - T_B(\mathbf{b}_B)\sigma_{NN}]^{B-n} \binom{A}{m} [T_A(\mathbf{b}_A)\sigma_{NN}]^m [1 - T_A(\mathbf{b}_A)\sigma_{NN}]^{A-m} . \end{aligned} \quad (23)$$

Using $t(\mathbf{b}) \simeq \delta(\mathbf{b})$ we get

$$\begin{aligned} P(n, m, \mathbf{b}_A, \mathbf{b}_B) &= \binom{A}{n} \binom{B}{n} [T_B(\mathbf{b}_B)\sigma_{NN}]^n [1 - T_B(\mathbf{b}_B)\sigma_{NN}]^{B-n} \\ &\times [T_A(|\mathbf{b} - \mathbf{b}_B|)\sigma_{NN}]^m [1 - T_A(|\mathbf{b} - \mathbf{b}_B|)\sigma_{NN}]^{A-m} . \end{aligned} \quad (24)$$

The abrasion-ablation model [11] used in Section 3 is based on this equation. It is extended to account for the isospin dependence of the nucleon-nucleon collisions in a trivial way. In that Section m is interpreted as the number of holes created in the nucleon orbitals in the target. These equations can also be derived quantum-mechanically using the *eikonal approximation*). This was shown by Hüfner, Schäfer and Schürman [17]. The derivation presented in this Supplement is much simpler and only requires the use of probability concepts.

3 Isotope yield in high energy collisions

Using the probability approach to high energy scattering, described in Supplement A, we can develop a simple model to calculate the isotopic yield in high energy collisions of heavy nuclei. This is known as the *abrasion-ablation* model.

According to Carlson, Mastroleo and Hussein [18], the differential primary yield can be written as the product of a density of states $\omega(\varepsilon, Z_f, A_f)$ and an integral

over impact parameter,

$$\begin{aligned} \frac{d\sigma_0}{d\varepsilon}(\varepsilon, Z_f, A_f) &= \omega(\varepsilon, Z_f, A_f) \\ &\times \int d^2b [1 - P_\pi(b)]^{Z_P - Z_f} P_\pi(b)^{Z_f} [1 - P_\nu(b)]^{N_P - N_f} P_\nu(b)^{N_f} . \end{aligned} \quad (25)$$

The integral gives the cross section for each primary fragment state as the sum over impact parameters of the probability that Z_f projectile protons and $N_f = A_f - Z_f$ projectile neutrons do not scatter, while the remaining ones do. The distinction between protons and neutrons generalizes the expression 5 of the Supplement A and permits one to account for the differences in their densities.

We can use Eq. 18 and write the probability that a projectile proton does *not* collide with the target as

$$\begin{aligned} P_\pi(b) &= \int d^2s dz \rho_\pi^P(z, \mathbf{s}) \\ &\times \exp \left[-\sigma_{pp} Z_T \int dz \rho_\pi^T(z, \mathbf{b} - \mathbf{s}) - \sigma_{pn} N_T \int dz \rho_\nu^T(z, \mathbf{b} - \mathbf{s}) \right] \end{aligned} \quad (26)$$

where ρ_π^P and ρ_ν^T are the projectile and target single-particle proton and neutron densities while σ_{pp} and σ_{pn} are the total (minus Coulomb) proton-proton and proton-neutron scattering cross sections, respectively. The neutron probability can be expressed likewise as

$$\begin{aligned} P_\nu(b) &= \int d^2s dz \rho_\nu^P(z, \mathbf{s}) \\ &\times \exp \left[-\sigma_{pn} Z_T \int dz \rho_\pi^T(z, \mathbf{b} - \mathbf{s}) - \sigma_{pp} N_T \int dz \rho_\nu^T(z, \mathbf{b} - \mathbf{s}) \right] \end{aligned} \quad (27)$$

where we have identified the total neutron-neutron scattering cross section σ_{nn} with the proton-proton one. At lower energies it is important to account for the Pauli blocking of the nucleon-nucleon scattering. This tends to reduce the values of σ_{NN} entering Eqs. 26 and 27. A geometrical model of Pauli blocking is discussed in Supplement B.

Note that Eqs. 25, 26 and 27 are slightly different than those that we have derived in Supplement A. The difference is the replacement of the probability $1 - T(\mathbf{b})\sigma_{NN}$ by $\exp[-T(\mathbf{b})\sigma_{NN}]$, to account for unitarity (i.e., when $T(\mathbf{b})\sigma_{NN}$ is larger than the unity). This form of the collision probability is often used in the literature. It can also be justified in terms of probabilistic concepts, as we will do

later, where we will introduce the “ $t\rho\rho$ ” approximation, useful to calculate total reaction cross sections (see also the arguments leading to Eq. 19).

For each primary fragment, the density of states, $\omega(\varepsilon, Z_f, A_f)$, is obtained by counting all combinations of projectile holes consistent with the fragment’s charge and neutron numbers. Each hole is a state left vacant by an abraded nucleon. One can use the projectile single-particle energies in the calculation since the mean field rearrangements that would modify them do not have time to occur until long after the abrasion stage has passed. The distribution is shifted down in energy so that the lowest level is at zero excitation energy (This ground level is obtained by removing the nucleons from the highest energy levels in the projectile.). The total number of states is given by

$$\mathcal{N}(Z_f, A_f) = \int d\varepsilon \omega(\varepsilon, Z_f, A_f) = \binom{Z_P}{Z_f} \binom{N_P}{N_f}. \quad (28)$$

Thus, the energy-integrated primary cross section contains the combinatorial factors $\binom{Z_P}{Z_f}$ and $\binom{N_P}{N_f}$.

A collision between two nuclei of zero isotopic spin, in which the proton and neutron distributions for each nucleus are taken to be identical, results in energy-integrated primary cross sections that are symmetric in charge and neutron number about the point $Z_f = N_f = A_f/2$. This need not be the case when the distributions are different or when one of the nuclei is not of zero isotopic spin. The calculations of Ref. [18], based on Eqs. 25 - 28, show that the asymmetry of the primary yield from a $Z = N$ projectile on a $Z \neq N$ target is small. The target dependence of the primary projectile yield is thus an almost purely geometrical one.

The primary yields in this model depend on the incident energy only through the nucleon-nucleon cross sections in the absorption factors of Eqs. 26, 27. At high energies ($E/A > 1$ GeV/nucleon), these cross sections have nearly the same value. We thus expect differences in proton and neutron scattering to be their smallest at such energies. Any differences will be seen best at lower energies where the proton-neutron cross section reaches values three times that of the proton-proton and neutron-neutron ones. The effects of this dependence are found to be small. The yields obtained in these calculations [18] are almost independent of the incident energy.

We show in Fig. 5(b) the results of Ref. [18] for the system $^{16}\text{O} + \text{Pb}$ and for the average excitation energy obtained from the densities of states as a function of the primary fragment mass A_f . The average was performed over all isotopes with a given A_f in order to remove the slight isotopic dependence of the individual averages. The distributions’ variance is displayed as an error bar on each point. Also shown, as a solid line in Fig. 5(b), is the excitation energy that would be obtained using a surface energy estimate [11]. The latter yields about half the average energy of the hole distribution but remains within its variance for all but the largest mass losses.

As can be seen in Fig. 5(b), the average excitation energy of fragments that undergo little abrasion remains below the particle emission threshold, although their

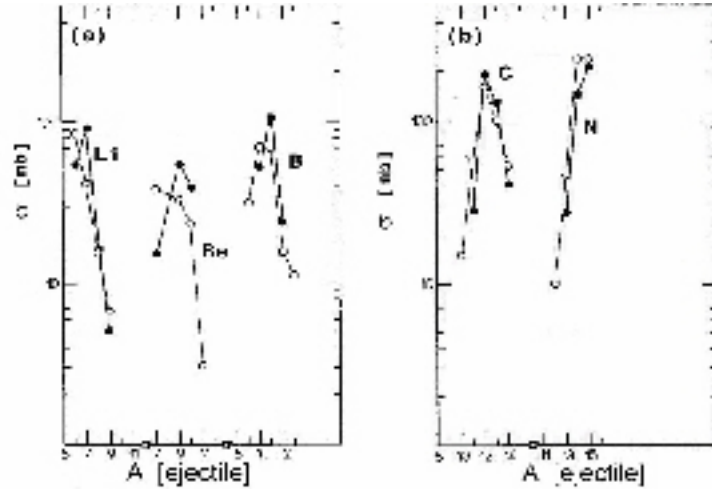


Figure 6 Calculated secondary yields in the reaction $^{16}\text{O} + ^{208}\text{Pb}$ at $E_{lab} = 20$ MeV/nucleon are shown as open circles for the isotopes of (a) lithium, beryllium, and boron, and (b) of carbon and nitrogen. The data of ref. [20] are shown as full circles.

energy distribution extends above it. In these cases, use of the energy distribution rather than an average value is essential for describing the decay.

One can resort to several statistical models to calculate the particle evaporation during the ablation stage as a function of the primary fragment charge Z_f , mass A_f , and excitation energy ε . For the calculations presented here the limiting Weisskopf-Ewing evaporation formalism was used [19]. The result of the evaporation calculation can be expressed as the probability, $P(Z, A; \varepsilon, Z_f, A_f)$, of yielding a residue of charge Z and mass A , given a primary compound nucleus of charge Z_f mass A_f and excitation energy ε . In terms of this quantity and the differential primary yield $d\sigma_0(\varepsilon, Z_f, A_f)/d\varepsilon$, one can calculate the observed secondary yield, $\sigma_0(Z, A)$, as

$$\sigma_0(Z, A) = \sum_{Z_f, A_f} \int d\varepsilon P(Z, A; \varepsilon, Z_f, A_f) \frac{d\sigma_0}{d\varepsilon}(\varepsilon, Z_f, A_f) \quad (29)$$

We show the calculation for $^{16}\text{O} + ^{208}\text{Pb}$ together with the experimental data [20, 21] at 20 MeV/nucleon and 2 GeV/nucleon in Figs. 6 and 7, respectively. In particular we note the agreement of the calculation with the projectile-like isotope data. The agreement with the data, especially that at 2 GeV/nucleon, is quite reasonable.

The microscopic calculation of the absorption probabilities and cross sections permits the use of more realistic collision geometries. A natural step in this direction is to next replace the average single-particle projectile densities in Eqs. 26 and 27 by the probability distributions of the individual projectile orbitals. This allows one to take into account differences in the abrasion probabilities or the different orbitals. In ^{16}O for example, we expect the removal of a p-orbital nucleon to be more likely than

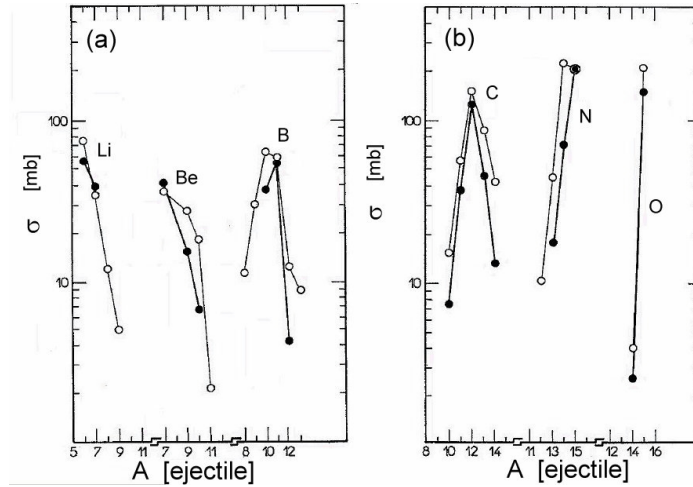


Figure 7 Calculated secondary yields in the reaction $^{16}\text{O} + ^{208}\text{Pb}$ at $E_{lab} = 2$ GeV/nucleon are shown as open circles for the isotopes of (a) lithium, beryllium, and boron and (b) of carbon, nitrogen, and oxygen. The data of ref. [21] are shown as full circles .

that of an s-orbital one, since the former will tend to be at a larger radius than the latter.

Thus generalized, the expression for the differential primary yield, $d\sigma_0(\varepsilon, Z_f, A_f) / d\varepsilon$, becomes a sum over all the possible combinations of orbital transmission and absorption factors that result in a given primary charge Z_f and mass A_f . The population of primary fragment states will no longer be evenly distributed but will depend on the absorption probabilities of the single-particle states on which they are based. As the nucleons that are less bound are the more superficial ones and, thus, also the ones more likely to be absorbed, the average primary fragment excitation energy will be lower in this more realistic model. The model presented in this Section shows that we can understand the main features of the isotopic fragmentation yield in heavy ion collisions at high energies in terms of simple Glauber calculations and with statistical decay models for the spectators and participants.

Later on we will discuss the production of exotic nuclei in fusion reactions and in Coulomb fission processes. Before that we will develop the tools we need to understand these processes.

Supplement B

4 Pauli blocking of nucleon-nucleon scattering

The main effect of medium corrections is due to the Pauli-blocking of nucleon-nucleon scattering. Pauli-blocking prevents the nucleons to scatter into final occupied states in

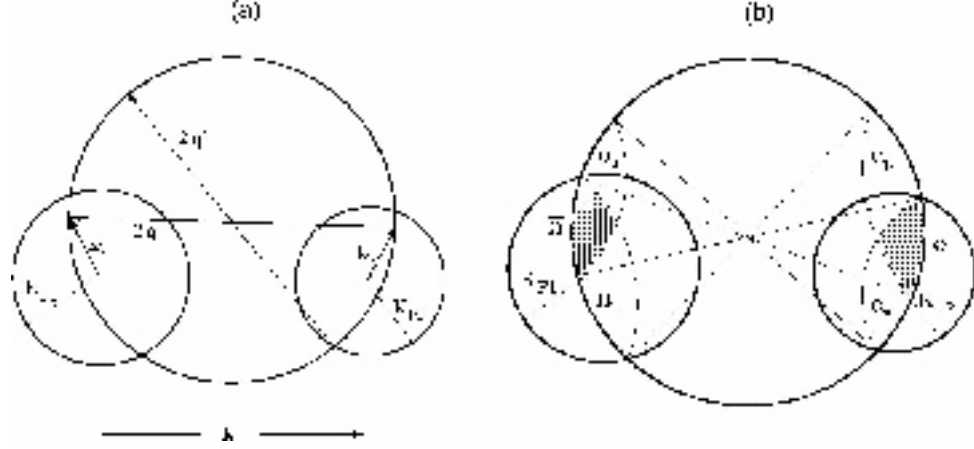


Figure 8 (a) A nucleon from inside a Fermi sphere scatters off a nucleon from another Fermi sphere. (b) Due to the Pauli principle the scattering angle of the nucleons is restricted to lie outside the Fermi spheres.

binary collisions between the projectile and target nucleons. This is best seen in momentum space, as shown in Fig. 8. We see that energy and momentum conservation, together with the Pauli principle, restrict the collision phase space to a complex geometry involving the Fermi-spheres and the scattering sphere.

In this scenario, the in-medium cross section corrected by Pauli-blocking can be defined as

$$\sigma_{NN}(k, K_{F1}, K_{F2}) = \int \frac{d^3k_1 d^3k_2}{(4\pi K_{F1}^3/3)(4\pi K_{F2}^3/3)} \frac{2q}{k} \sigma_{NN}^{free}(q) \frac{\Omega_{Pauli}}{4\pi}, \quad (30)$$

where \mathbf{k} is the relative momentum per nucleon of the nucleus-nucleus collision (see figure 8), and $\sigma_{NN}^{free}(q)$ is the free nucleon-nucleon cross section for the relative momentum $2\mathbf{q} = \mathbf{k}_1 - \mathbf{k}_2 - \mathbf{k}$, of a given pair of colliding nucleons. Clearly, Pauli-blocking enters through the restriction that $|\mathbf{k}'_1|$ and $|\mathbf{k}'_2|$ lie outside the Fermi spheres. From energy and momentum conservation in the collision, \mathbf{q}' is a vector which can only rotate around a circle with center at $\mathbf{p} = (\mathbf{k}_1 + \mathbf{k}_2 + \mathbf{k})/2$. These conditions yield an allowed scattering solid angle given by [22]

$$\Omega_{Pauli} = 4\pi - 2(\Omega_a + \Omega_b - \bar{\Omega}), \quad (31)$$

where Ω_a and Ω_b specify the excluded solid angles for each nucleon, and $\bar{\Omega}$ represents the intersection angle of Ω_a and Ω_b (see Fig. 8).

The solid angles Ω_a and Ω_b are easily determined. They are given by

$$\Omega_a = 2\pi(1 - \cos \theta_a), \quad \Omega_b = 2\pi(1 - \cos \theta_b), \quad (32)$$

where \mathbf{q} and \mathbf{p} were defined above, $\mathbf{b} = \mathbf{k} - \mathbf{p}$, and

$$\cos \theta_a = (p^2 + q^2 - K_{F1}^2)/2pq, \quad \cos \theta_b = (b^2 + q^2 - K_{F2}^2)/2bq, \quad (33)$$

The evaluation of $\bar{\Omega}$ is tedious but can be done analytically. The full calculation was done by Bertulani [22] and the results have been reproduced in the Appendix of Ref. [23] (see also [24]). To summarize, there are two possibilities:

$$(1) \quad \bar{\Omega} = \Omega_i(\theta, \theta_a, \theta_b) + \Omega_i(\pi - \theta, \theta_a, \theta_b) , \quad \text{for } \theta + \theta_a + \theta_b > \pi \quad (34)$$

$$(2) \quad \bar{\Omega} = \Omega_i(\theta, \theta_a, \theta_b) , \quad \text{for } \theta + \theta_a + \theta_b \leq \pi , \quad (35)$$

where θ is given by

$$\cos \theta = (k^2 - p^2 - b^2)/2pb . \quad (36)$$

The solid angle Ω_i has the following values

$$(a) \quad \Omega_i = 0 , \quad \text{for } \theta \geq \theta_a + \theta_b \quad (37)$$

$$(b) \quad \Omega_i = 2 \left[\cos^{-1} \left(\frac{\cos \theta_b - \cos \theta \cos \theta_a}{\sin \theta_a (\cos^2 \theta_a + \cos^2 \theta_b - 2 \cos \theta \cos \theta_a \cos \theta_b)^{1/2}} \right) \right. \\ \left. + \cos^{-1} \left(\frac{\cos \theta_a - \cos \theta \cos \theta_b}{\sin \theta_b (\cos^2 \theta_a + \cos^2 \theta_b - 2 \cos \theta \cos \theta_a \cos \theta_b)^{1/2}} \right) \right. \\ \left. - \cos \theta_a \cos^{-1} \left(\frac{\cos \theta_b - \cos \theta \cos \theta_a}{\sin \theta \sin \theta_a} \right) \right. \\ \left. - \cos \theta_b \cos^{-1} \left(\frac{\cos \theta_a - \cos \theta \cos \theta_b}{\sin \theta \sin \theta_b} \right) \right] \quad (38)$$

$$\text{for } |\theta_b - \theta_a| \leq \theta \leq \theta_a + \theta_b , \quad (39)$$

$$(c) \quad \Omega_i = \Omega_b \quad \text{for } \theta_b \leq \theta_a, \theta \leq |\theta_b - \theta_a| , \quad (40)$$

$$(d) \quad \Omega_i = \Omega_a \quad \text{for } \theta_a \leq \theta_b, \theta \leq |\theta_b - \theta_a| , \quad (41)$$

The integrals over \mathbf{k}_1 and \mathbf{k}_2 in Eq. 30 reduce to a five-fold integral due to cylindrical symmetry. Two approximations can be done which greatly simplify the problem: (a) on average, the symmetric situation in which $K_{F1} = K_{F2} \equiv K_F$, $q = k/2$, $p = k/2$, and $b = k/2$, is favored, (b) the free nucleon-nucleon cross section can be taken outside of the integral in Eq. 30.

Both approximations are supported by the studies of Refs. [23] and have been verified numerically [22]. The assumption (a) implies that $\Omega_a = \Omega_b = \bar{\Omega}$, which can be checked using Eq. 41. One gets from 31 the simple expression

$$\Omega_{Pauli} = 4\pi - 2\Omega_a = 4\pi \left(1 - 2 \frac{K_F^2}{k^2} \right) . \quad (42)$$

Furthermore, the assumption (b) implies that

$$\sigma_{NN}(k, K_F) = \sigma_{NN}^{free}(k) \frac{\Omega_{Pauli}}{4\pi} = \sigma_{NN}^{free}(k) \left(1 - 2 \frac{K_F^2}{k^2} \right) . \quad (43)$$

The above equation shows that the in-medium nucleon-nucleon cross section is about 1/2 of its free value for $k = 2K_F$, i.e., for $E/A \simeq 150$ MeV, in agreement with the numerical

results of Ref. [23]. Since the effect of Pauli blocking at these energies is very large it is important to calculate the in-medium nucleon-nucleon scattering cross section according to Eq. 30, including the energy dependence of the free nucleon-nucleon cross sections.

The connection with the nuclear densities is accomplished through the local density approximation, which relates the Fermi momenta to the local densities as

$$K_F^2 = \left[\frac{3\pi}{4} \rho(r) \right]^{2/3} + \frac{5}{2} \xi (\nabla \rho / \rho)^2 \quad (44)$$

where $\rho(r)$ is the sum of the nucleon densities of each colliding nucleus at the position r .

The second term is small and amounts to a surface correction, with ξ of the order of 0.1 [23]. Inserting Eq. 44 into Eq. 43, and using $E = \hbar^2 k^2 / 2m_N$, one gets [24] (with $\bar{\rho} = \rho / \rho_0$)

$$\sigma_{NN}(E, \rho) = \sigma_{NN}^{free}(E) (1 + \alpha' \bar{\rho}^{2/3}) \quad \text{with} \quad \alpha' = -\frac{48.4}{E \text{ (MeV)}} \quad (45)$$

where the second term of Eq. 44 has been neglected. This equation shows that the local density approximation leads to a density dependence proportional to $\bar{\rho}^{2/3}$. The Pauli principle yields a $1/E$ dependence on the bombarding energy. This behavior arises from a larger phase space available for nucleon-nucleon scattering with increasing energy.

The nucleon-nucleon cross section at $E/A \lesssim 200$ MeV decreases with E approximately as $1/E$. We thus expect that, in nucleus-nucleus collisions, this energy dependence is flattened by the Pauli correction, i.e., the in-medium nucleon-nucleon cross section is less dependent of E , for $E \lesssim 200$, than the free cross section.

For higher values of E the Pauli blocking is less important and the free and in-medium nucleon-nucleon cross sections are approximately equal. These conclusions are in agreement with the experimental data for nucleus-nucleus reaction cross sections [25], and is explained in Ref. [23].

Notice that, for $E/A = 100 - 200$ MeV, and $\rho \simeq \rho_0$, Eq. 45 yields a coefficient α' between -0.2 and -0.5 . Values of α' between -0.2 and -0.4 were indeed obtained with more elaborate calculations using realistic nucleon-nucleon interactions [26].

5 References

1. I. Tanihata, on “*Treatise on Heavy-Ion Science*”, Vol. 8, Ed. by D. Allan Bromley, (Plenum Publ., 1989).
2. C. Détraz and D.J. Vieira, *Ann. Rev. Nucl. Part. Sci.* **39** (1989) 407.
3. E. Roeckel, *Rep. Prog. Phys.* **55** (1992) 1661.
4. A.C. Mueller and B.M. Sherill, *Ann. Rev. Nucl. Part. Sci.* **43** (1993) 529
5. C.A. Bertulani, L.F. Canto, and M.S. Hussein, *Phys. Rep.* **226** (1993) 281.
6. M.V. Zhukov, B.V. Danilin, D.V. Fedorov, J.M. Bang, I.J. Thompson and J.S. Vaagen, *Phys. Rep.* **231** (1993) 231.

7. H. Geissel, G. Muenzenberg and K. Riisager, *Ann. Rev. Nucl. Part. Sci.* **45** (1995) 163.
8. P.G. Hansen, A.S. Hansen, and B. Jonson, *Ann. Rev. Nucl. Part. Sci.* **45** (1995) 591.
9. I. Tanihata et al., *Phys. Rev. Lett.* **55** (1985) 2676.
10. K. Sümmerer and B. Blank, *Phys. Rev.* **C61** (2000) 034607.
11. J. D. Bowman, W. J. Swiatecki and C. F. Tsang, LBL Report LBL-2908, 1973 (unpublished).
12. L.F. Oliveira, R. Donangelo, and J.O. Rasmussen, *Phys. Rev.* **C19** (1979) 826.
13. J. Gosset , H. H. Gutbrod, W. G. Meyer, A. M. Poskanzer, A. Sandoval, R. Stock, and G. D. Westfall, *Phys. Rev.* **C16** (1977) 629.
14. W.A. Friedman, *Phys. Rev.* **C27** (1983) 569.
15. W.A. Friedman and W. Lynch, *Phys. Rev.* **C28** (1983) 950.
16. J.-J. Gaimard and K.-H. Schmidt, *Nucl. Phys.* **A531** (1991) 709.
17. J. Hüfner, K. Schäfer, and B. Schürmann, *Phys. Rev* **C12** (1975) 1888.
18. B.V. Carlson, R.C. Mastroleo, and M.S. Hussein, *Phys. Rev.* **C46** (1992) R30.
19. V.F. Weisskopf and D. H. Ewing, *Phys. Rev.* **57** (1940) 472; *ibid.* **57** (1940) 935.
20. C. Gelbke, C. Olmer, M. Buenerd, D.L. Hendrie, J. Mahoney, M.C. Mermaz, and D. K. Scott, *Phys. Rep.* **42** (1978) 312.
21. M. Buenerd, C. K. Gelbke, B. G. Harvey, D. L. Hendrie, J. Mahoney, A. Menchaca-Rocha, C. Olmer, and D. K. Scott, *Phys. Rev. Lett.* **37** (1976) 1191.
22. C.A. Bertulani, *Braz. J. Phys.* **16** (1986) 380.
23. M.S. Hussein, R.A. Rego, and C.A. Bertulani, *Phys. Rep.* **201** (1991) 279.
24. C.A. Bertulani, *J. Phys.* **G27** (2001) L67.
25. S. Kox, A. Gamp, C. Perrin, J. Arvieux, R. Bertholet, J.F. Bruandet, M. Buenerd, Y. El Masri, N. Longequeue, and F. Merchez, *Phys. Lett.* **B159**, (1985) 15.
26. T. Alm, G. Röpke, W. Bauer, F. Daffin, and M. Schmidt, *Nucl. Phys.* **A587** (1995) 815; A. Schnell, G. Röpke, U.Lombardo, and H-J. Schulze, *Phys. Rev.* **C57** (1998) 806.